PRAMANA — journal of physics

Vol. 78, No. 4
April 2012
pp. 635–649

Thermal conductivity of large-grain niobium and its effect on trapped vortices in the temperature range 1.8–5 K

J MONDAL[1,*], G CIOVATI[2], K C MITTAL[1] and G R MYNENI[2]
[1]Accelerator and Pulse Power Division, Bhabha Atomic Research Centre, Trombay, Mumbai 400 085, India
[2]Jefferson Lab, 12000 Jefferson Ave, Newport News, VA 23606, USA
*Corresponding author. E-mail: jmondal@barc.gov.in

MS received 30 April 2011; revised 9 November 2011; accepted 8 December 2011

Abstract. Experimental investigation of the thermal conductivity of large grain and its dependence on the trapped vortices in parallel magnetic field with respect to the temperature gradient ∇T was carried out on four large-grain niobium samples from four different ingots. The zero-field thermal conductivity measurements are in good agreement with the measurements based on the theory of Bardeen–Rickayzen–Tewordt (BRT). The change in thermal conductivity with trapped vortices is analysed with the field dependence of the conductivity results of Vinen *et al* for low inductions and low-temperature situation. Finally, the dependence of thermal conductivity on the applied magnetic field in the vicinity of the upper critical field H_{c2} is fitted with the theory of pure type-II superconductor of Houghton and Maki. Initial remnant magnetization in the sample shows a departure from the Houghton–Maki curve whereas the sample with zero trapped flux qualitatively agrees with the theory. A qualitative discussion is presented explaining the reason for such deviation from the theory. It has also been observed that if the sample with the trapped vortices is cycled through T_c, the subsequent measurement of the thermal conductivity coincides with the zero trapped flux results.

Keywords. Niobium; thermal conductivity; phonon; trapped flux.

PACS Nos 74.25.fc; 74.25.Kc; 74.25.Op

1. Introduction

Niobium is the material of choice for superconducting radiofrequency (SRF) cavity programs in different particle accelerator laboratories because of its mechanical properties are favourable for formability, machining and also because of its high T_c and high first flux penetration field H_{c1}. SRF cavity performances have been continually improved for the past three decades to achieve a reproducible quality factor of 10^{10} and accelerating fields (E_{acc}) of 30–35 MV/m. The present approach for the fabrication of superconducting radiofrequency (SRF) cavities is to roll and deep draw sheets of polycrystalline high-purity niobium. Jefferson Laboratory pioneered the use of large-grain/single-crystal

Nb directly sliced from an ingot for the fabrication of single-crystal high-purity Nb SRF cavities [1]. The large-grain/single-crystal niobium has several potential advantages over the polycrystalline niobium as discussed in ref. [2] and has become a viable alternative to the standard fine grain (ASTM grain size > 6), high purity (RRR ≥ 250) niobium for the fabrication of high-performance SRF cavities for particle accelerators. A cavity made of large-grain or single-crystal niobium operating below 2 K may have a better thermal stability due to the reduction of phonon scattering by grain boundaries (causing the so-called 'phonon peak'). Many measurements have shown that the scattering of phonons and electrons with the fluxoids decreases the observed thermal conductivity [3,4]. For instance, at low temperature ($T \ll T_c$), for niobium between the temperature 3–1.8 K, K_{ph} montonically increases due to the decrease of scattering of phonons with the electrons because of the electron decoupling resulting from the condensation into Cooper pairs. The thermal conductivity in the mixed state, have been measured in previous studies [3–7]. They showed that with the increasing magnetic field in the mixed state, more and more fluxoids enter the superconductor and as a result both electron and phonon mean-free paths (mfp) decrease. This article presents results on the thermal conductivity measurement of large-grain niobium in the Meissner state and in the mixed state in the temperature range 1.8–5 K and for magnetic fields up to the surface critical field, H_{c3}. Also the effect of initial trapped vortices on the Meissner and mixed state conductivity of type-II superconductor is studied here. The results show that when the sample is cycled through T_c, with no external field applied, the sample re-gain the Meissner state and the thermal conductivity has the same value as with no trapped flux. The zero-field thermal conductivity data have been fitted with the semiempirical parametrization of Koechlin and Bonin [8]. The results for the specimen with the trapped vortices are interpreted with phonon-vortex scattering, using the qualitative model of Vinen *et al* [4]. The thermal conductivity as a function of B in the mixed state is analysed using the Houghton–Maki theory [9].

2. Experimental set-up

2.1 *System design*

A system to measure the magnetization curve and the thermal conductivity of the cylindrical sample rod of 6 mm diameter and 120 mm length was designed and built. Figure 1 shows a schematic of the system and the picture of the sample rod. A heater made with constantan wire glued on a Cu block with epoxy is clamped near the base of the sample. Two calibrated Cernox resistors are soldered with indium on two small Cu blocks which are clamped to the rod at a distance of about 40 mm. A pickup coil (< 200 turns, 0.29 mm diameter Cu wire) is inserted in the middle of the sample, between the two Cernox resistors. The sample is clamped on a Cu block which is inserted in a copper tube and sealed with indium wire. A stainless steel $2\frac{3}{4}$ Conflat flange was brazed on the other end of the tube. The tube is bolted to a 'T' section where a flange with feed-through connectors is bolted on the side. The assembly is bolted to the vacuum line on a vertical test stand (the pressure in the Cu tube is $<$10–5 mbar at 4.3 K). Some heat shields are inserted in the vacuum line to minimize radiation losses. A superconducting magnet up to 1 T (0.1%

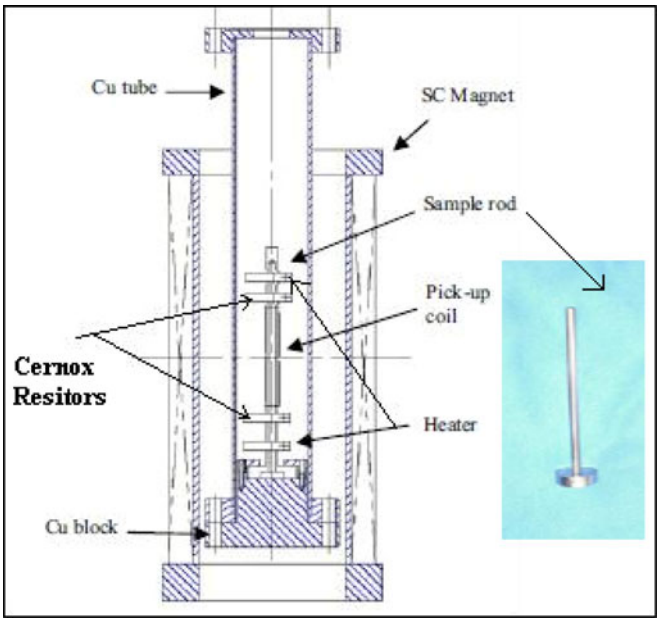

Figure 1. Schematic of the system for measuring the superconducting properties of the sample and a picture of the sample rod.

field homogeneity over the sample length) made by cryomagnetics surrounds the Cu tube carrying the sample.

2.2 *Measurement methods*

The thermal conductivity as a function of the average temperature of the sample is calculated using Fourier's law where the power supplied to the heater, P, the temperature difference, ΔT, the distance d between the two Cernox, and the cross-sectional area of the sample A are measured:

$$K = \frac{P}{\Delta T}\frac{d}{A}. \tag{1}$$

The heater power and the sample temperature are controlled with a LakeShore 332 Temperature Controller.

The magnetization of the sample as a function of the applied field is obtained by linearly ramping the current in the superconducting magnet (the field-to-current ratio is 12.9 mT/A) at a rate of about 0.1 A/s while measuring the voltage from the pick-up coil with a Keithley 2182 nanovoltmeter. The magnetization is calculated using the following formula [10]:

$$M(B_a) = \frac{-1}{1 - N_{\mathrm{D}}}\int_0^{B_a} \frac{V(B'_a) - V_{\mathrm{n}}}{V_{\mathrm{s}} - V_{\mathrm{n}}}\mathrm{d}B'_a, \tag{2}$$

where V_{n} and V_{s} are the voltages in the normal and superconducting state respectively and N_{D} is the demagnetization factor, estimated to be about 0.007 for our samples. A Power

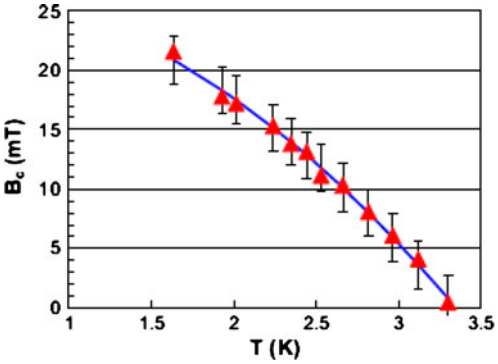

Figure 2. Critical magnetic field as a function of temperature measured on an indium rod of 99.99% purity. The solid line is a least-square fit with eq. (3).

Ten power supply (0–10 V, 0–100 A) controlled by an American Magnetics 412 Programmer, remotely controlled by a PC, provides current to the superconducting solenoid. For calibration purposes, we also measured the critical field B_c as a function of temperature for an indium rod (99.99% purity) made by melting indium in a stainless steel mold. The data, showed in figure 2, are fitted with the classical formula

$$B_c(T) = B_c(0)\left(1 - \frac{T^2}{T_c^2}\right) \tag{3}$$

and resulted in $T_c = 3.35 \pm 0.03$ K and $B_c(0) = 27 \pm 2$ mT, are in good agreement with the published data [11].

3. Zero-field temperature dependence of the thermal conductivity

The thermal conductivity K is the sum of contributions from electrons and phonons, $K = K_{es} + K_{latt.}$. The electron heat conduction in the superconducting state is reduced because the electrons which have condensed into Cooper pairs do not contribute to any disorder or entropy transport any more. The remaining fraction of electrons which contribute to heat transport decreases exponentially with decreasing temperature. According to BRT theory [8,12],

$$\frac{K_{es}}{K_{en}} = R(y), \quad R(y) \leq 1, \tag{4}$$

where

$$R(y) = (f(0))^{-1}\left[f(-y) + y\ln(1+\exp(-y)) + y^2/\left(2\left(1+\exp(y)\right)\right)\right]$$

and

$$y = \frac{\Delta(T)}{K_B T} = \left(\frac{\Delta(T)}{K_B T_c}\right)\left(\frac{T_c}{T}\right).$$

The approximation $y \cong \alpha T_c/T$ is valid if $T/T_c \leq 0.6$. Finally $f(-y)$ is defined as

$$f(-y) = \int_0^\infty \frac{z\,dz}{1+\exp(z+y)}, \quad \text{with } f(0) = \pi^2/12.$$

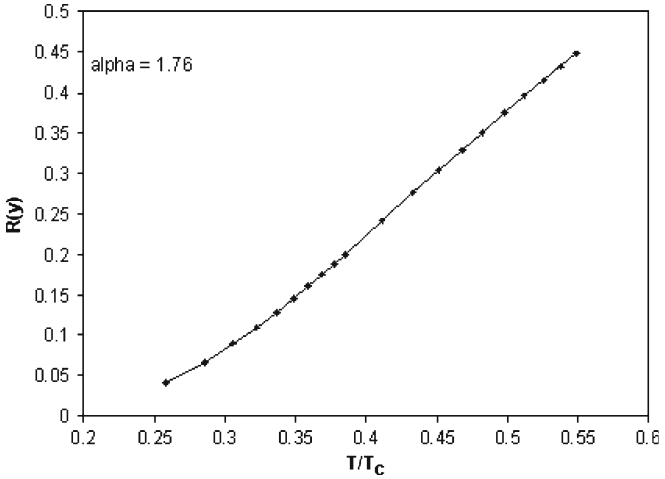

Figure 3. The ratio of $K_{es}/K_{en} = R(y)$ as a function of reduced temperature, $T/T_c = \alpha/y$ (within the experimental temperature range).

Here, T_c is the critical temperature of the superconductor, $\Delta(T)$ is the superconductor energy gap and $\alpha \approx 1.76$ in the BCS theory, but may take values in the range $1.75 \leq \alpha \leq 1.95$ because of strong coupling effects. The ratio $K_{es}/K_{en} = R(y)$ is plotted as a function of T/T_c taking $\alpha \approx 1.76$ in figure 3 within the experimental temperature range 1.8–5 K used in our experiments.

The lattice thermal conductivity is limited by the different scattering mechanisms of phonons with point defects, dislocations (line defects), grain boundaries, sample walls and electrons. The general expression for lattice conductivity is $K_{\text{latt.}} = \frac{1}{3}C_v \cdot v^2 \cdot \tau$ where $1/\tau$ is the total scattering rate of phonons from different scattering mechanisms, C_v is the specific heat per unit volume and v is the average velocity of the carriers of thermal energy. The resultant lattice thermal conductivity, taking into account the phonon scattering by the electrons and by the crystal boundaries, is given by

$$K_{\text{latt.,s}} \cong \left[\frac{1}{\exp(y)DT^2} + \frac{1}{Bl_{\text{ph}}T^3}\right]^{-1}, \tag{5}$$

where D and B are two constants and l_{ph} is the phonon mean-free path and for our large-grain niobium sample it is the smallest sample dimension as the grain size of the sample is bigger than the diameter of the sample rod. The total heat conductivity of the superconducting metal is obtained by adding the electron term $K_{es}(T)$ and the lattice term $K_{\text{latt.,s}}(T)$. This of course is valid for temperatures T lower than the critical temperature, because $y = \Delta(T)/K_B T$ is defined only in this domain,

$$K_s(T) \cong R(y)\left[\frac{\rho_{295\,\text{K}}}{L \cdot \text{RRR} \cdot T} + A \cdot T^2\right]^{-1} + \left[\frac{1}{\exp(y)DT^2} + \frac{1}{BlT^3}\right]^{-1}, \tag{6}$$

where L is the Lorentz constant, A is the coefficient of momentum exchange with lattice vibrations, D is the coefficient of momentum exchange with the normal electrons and B is a constant which depends on the material and mechanism of scattering. In order to obtain

$K_s(T)$ using this model, it is necessary to give experimental values to three variables: temperature T, residual resistivity ratio RRR and the phonon mean-free path l_{ph}. On the other hand, the theoretical parameters A, L, α, B and D are obtained by fitting these five parameters to the experimental results. The RRR value is generally determined by the well-known relationship established by Padamsee *et al* [13], RRR $= 4K_{s,4.2\,K}$. But to determine the RRR value in our studies we have measured the thermal conductivity at 4.2 K in normal (K_{en}) and superconducting states (K_{es}) and then used the following procedure to have the correct value of the measured RRR. The standard formula of RRR is replaced by RRR $= \delta K_{s,4.2\,K}$, where δ is defined by $\delta = \rho_{295\,K}/R(y)LT$. To calculate the RRR value we take $\rho_{295\,K} = 1.44 \times 10^{-7}$ Ω-m, $L = 2.45 \times 10^{-8}$ W K^{-2}, $T = 4.2$ K and $R(y)$ is experimentally determined using eq. (4). It is found that $\delta = 4.7$ for BCP cleaned samples whereas for the heat treated samples it varied from 4.2 to 4.5.

Figures 4 and 5 show experimental thermal conductivity measurement data for four different samples named A0, B0, C0 and D0 in figure 4 and A1, B1, C1 and D1 in figure 5. The corresponding RRR values are shown in the insets of figures 4 and 5. The samples A0, B0, C0 and D0 are degreased ultrasonically after the EDM wire cut and then about 180 μm are etched away from all the samples surfaces by buffered chemical polishing (BCP – 1 : 1 : 1, HF+HNO_3+H_3PO_4). After the first set of measurements, all the samples are degassed in a vacuum furnace at 600°C for 10 h in a vacuum better than 10^{-6} Torr. Then a light BCP (1(HF) : 1(HNO_3) : 2(H_3PO_4)) is carried out on all the heat treated samples to remove about 20 μm. This set of samples is named A1, B1, C1 and D1 respectively. The experimental curves are fitted with the above model taking $L = 2.45 \times 10^{-8}$ W K^{-2} and the theoretical parameters A, α, B and D obtained from the fitting curves are listed in table 1.

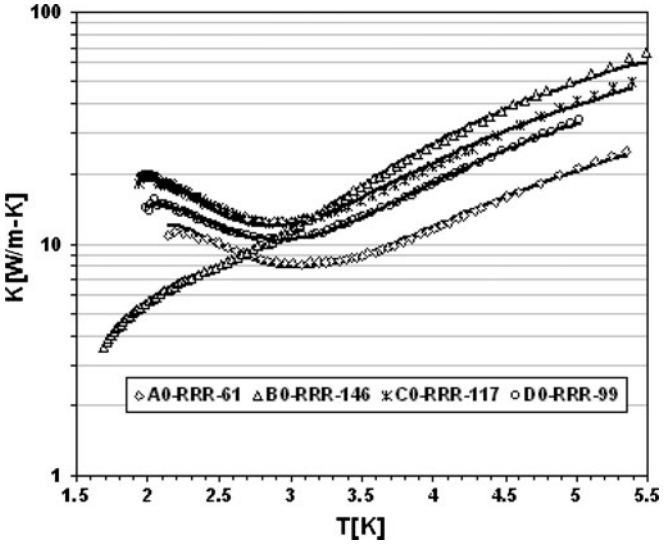

Figure 4. Experimental thermal conductivity data for 180 μm buffered chemical polished niobium samples from four different ingots. Solid lines are the fitting curves.

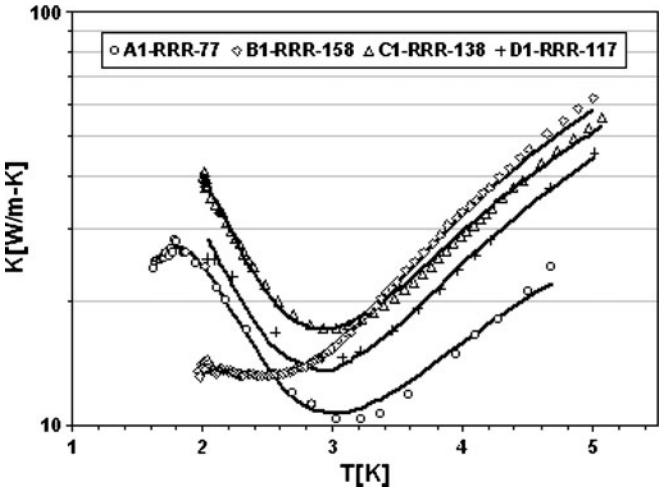

Figure 5. Experimental thermal conductivity data for 600°C heat treated niobium samples from four different ingots. Solid lines are the fitting curves.

The resultant error in K calculation is $\langle(\Delta K/K)^2\rangle^{1/2} \cong 6\%$. The experimental fit parameters are in good agreement with theoretical parameters reported in ref. [8]. Table 1 shows that the BCS gap parameter α does not change in all four samples before and after the 600°C degassing. The 600°C, 10 h degassing is given to remove interstitial hydrogen and for mechanical stress relaxation. Thus 600°C degassing has no effect on the BCS electron–phonon coupling constant, $\lambda \sim N(\varepsilon_F) \cdot V$, where $N(\varepsilon_F)$ is the density of states for normal electrons at Fermi energy and V is the matrix element of scattering interaction. It suggests that another scattering mechanism such as electron defect is responsible for the change in thermal conductivity after 600°C heat treatment. The parameter $B \propto 1/a_0$ increases after the degassing, where a_0 is the lattice constant. The increase in B implies that the lattice constant a_0 decreases and hence the interstitial hydrogen concentration decreases which plays a role in the lattice parameter expansion when it is trapped at the tetrahedral positions of the BCC niobium lattice.

Table 1. Theoretical fitting parameters of the thermal conductivity data.

	Parameters			
Samples	α	A	$1/D$	B
A0	1.87	5.03E−05	482	1.02E+03
B0	1.78	3.05E−05	523	3.78E+02
C0	1.81	4.07E−05	348	2.02E+03
D0	1.86	2.97E−05	423	1.24E+03
A1	1.86	1.00E−05	402	3.01E+03
B1	1.77	7.00E−07	299	1.06E+03
C1	1.80	1.00E−06	237	6.32E+03
D1	1.86	1.64E−05	289	2.33E+03

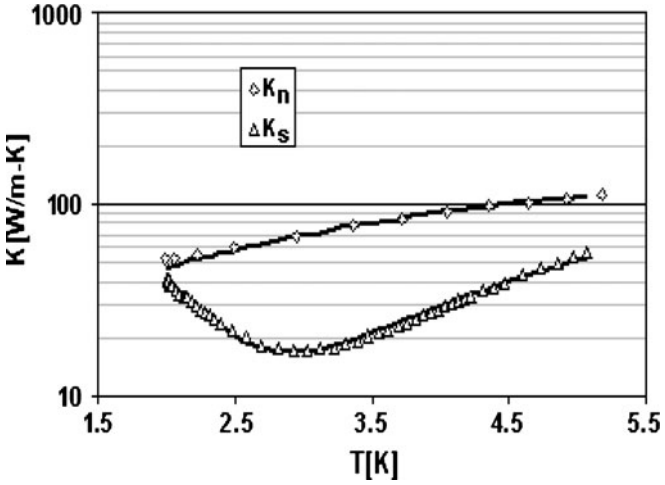

Figure 6. Thermal conductivity data in normal and superconducting states for the sample C1. Solid lines are the fitting curves with eq. (6).

The temperature dependence of thermal conductivity for sample C1 in the superconducting state K_s and the normal conducting state K_n is plotted in figure 6. The solid line which fits the normal state data points is obtained from the first term on the right-hand side of eq. (6) excluding the $R(y)$ term. The parameter A is the best fit value as shown in table 1 for the sample C1 and $L = 2.45 \times 10^{-8}$ W K^{-2}, $\rho_{295\,\mathrm{K}} = 1.45 \times 10^{-7}$ and RRR = 138 are used as material constants for the fit in superconducting state. So the fit parameters are in good agreement for both the normal state and superconducting state data. As a result, this model can be used to calculate the electronic and phonon conductivities in normal and superconducting states.

4. Field dependence of thermal conductivity

The core of the trapped flux line is represented by a region of radius ξ, the GL coherence length, within which the modulus of the order parameter, $\Delta(r)$, is appreciably reduced. Within this core, the magnetic field and the superfluid velocity are large enough to cause depairing, so that we expect to find bound excitations that are localized within the core. From the studies of Caroli *et al* [14], for clean materials with large GL parameter k, it is confirmed that except for an energy gap $\sim \Delta_\infty/E_\mathrm{F}$, where Δ_∞ is the BCS energy gap in the Meissner state and E_F is the Fermi energy, the density of states is similar to that in a normal metal cylinder of radius ξ. The effect of magnetic field in the materials of smaller k_GL (λ_L/ξ) has been studied by Hansen [15] and by Bergk and Tewordt [16]. They found that the small gap may disappear, but the density of states remains of the same order of magnitude.

The properties of these excitations (for small and large k_GL) are quite different from those of normal electrons: coherence factors are generally different, and group velocities along the flux lines are expected to be much smaller than those of the normal electrons.

The low group velocity means that the contribution of the bound excitations to the thermal conductivity (measured parallel to the flux lines) should be very small. In addition to these bound excitations there will be unbound excitations. The unbound excitations behave as BCS quasiparticles at distances larger than the penetration depth from the vortex core. Near the flux lines they will be modified as they interact with the magnetic field, the superfluid velocity and the modulation of $\Delta(r)$. This interaction will cause scattering among quasiparticles which in turn will reduce the electronic thermal conductivity in the mixed state due to the trapped flux lines in the material at favourable locations. In the Meissner state, phonons interact with the electronic excitations, and this interaction plays an important role in thermal conduction in the Meissner state of a superconductor at fairly low temperatures. When the magnetic flux is trapped within the material, phonons will again interact with the bound excitations in the core. The strength of this interaction can be calculated from Caroli *et al* [14] taking into account much higher frequencies for the thermally excited phonons.

Before presenting the experimental results, a theoretical review of the field dependence of the phonon and electron conductivities is discussed below.

(i) At low inductions ($H \ll H_{c2}$) and at low temperature ($T \ll T_c$) the phonons are scattered by a random array of vortices and these behave as if they were cylinders of normal metal [9,15]. The qualitative expression of the phonon conductivity as a function of B is given by

$$\frac{K_{ph}(0)}{K_{ph}(B)} = 1 + \sigma \frac{B}{H_{c2}} \frac{K_{ph}(0)}{K_{ph}^{n}}, \tag{7}$$

where σ is the average scattering diameter of the vortex line for the thermal phonons ($\sigma \sim 0.5$). Similarly, the electronic thermal conductivity as a function of B is given by

$$\frac{K_e(0)}{K_e(B)} = 1 + \frac{l_e a B}{\Phi_0}, \tag{8}$$

where l_e is the mean-free path of electrons in zero field, Φ_0 is the flux quanta and a is the effective scattering diameter of a vortex line for the free excitations.

(ii) At large inductions, i.e. close to H_{c2} and at low temperature, the field-dependent thermal conductivity has been analysed by Houghton and Maki [9]. They have determined the thermal conductivity when (a) the temperature gradient is parallel to the applied magnetic field and (b) the temperature gradient is perpendicular to the applied magnetic field. The result of Houghton and Maki for the temperature gradient parallel to the applied magnetic field is given by

$$\frac{\Delta K_{\parallel}}{K_e^{n}} = -6\mu \left[\left(1 - \mu^2\right) J_1 - \left(\frac{1}{4}\pi - \mu \right) \right], \tag{9}$$

where

$$J_1 = \int_0^{\pi/2} \frac{\cos\theta}{\cos\theta + \mu} \mathrm{d}\theta = \frac{\pi}{2} + \frac{2\mu}{\sqrt{1-\mu^2}} \tanh^{-1} \left[\frac{\mu - 1}{\sqrt{1-\mu^2}} \right]$$

and μ is the transport coefficient given by

$$\mu = 2\sqrt{\pi}\frac{\Delta^2}{\hbar^2 k_c v_F^2} l_e$$

in which k_c is the reciprocal lattice vector of the vortex lattice, v_F is the Fermi velocity, Δ is the order parameter, l_e is the electron mean-free path and $\Delta K_{\parallel}$ is the difference between the normal and superconducting state electronic thermal conductivities.

Figure 7 shows the experimental thermal conductivity measurement of the samples A1 and C1 with and without the trapped vortices. The bulk magnetization measurement allows us to get the values of remnant magnetization for those samples.

The bulk magnetization measurement for A1 and C1 is shown in figure 8. The magnetization curves show that the trapped magnetic fluxes in A1 and C1 are 58 and 80 mT respectively. Figure 7 shows that the effect on the electronic part of the thermal conductivity by the scattering of electrons with the vortex cores is negligibly small, whereas the phonons are strongly scattered causing an almost zero contribution to the net thermal conductivity. The field dependence of phonon and electronic conductivities of eqs (7) and (8) are used to interpret the thermal conductivity results with trapped vortices for the samples A1 and C1. K_{ph}^{n} is calculated from eq. (5) for normal metals using the value of the parameters D and B from table 1. The phonon conductivities in the normal state for A1 and C1 are 0.01 and 0.017 W/m-K respectively. The value of electron mfp, l_e, is calculated using the expression $(1/\rho) = 2e^2 S_F l_e/3(2\pi\hbar)^3$, where S_F is the area of the Fermi surface in momentum space in the first Brillouin zone and ρ is the electrical resistivity. The values $S_F = 2.23 \times 10^{-47}$ kg^2 m^2/s^2, $\rho = 2.37 \times 10^{-9}$ and 1.12×10^{-9} Ω-m are

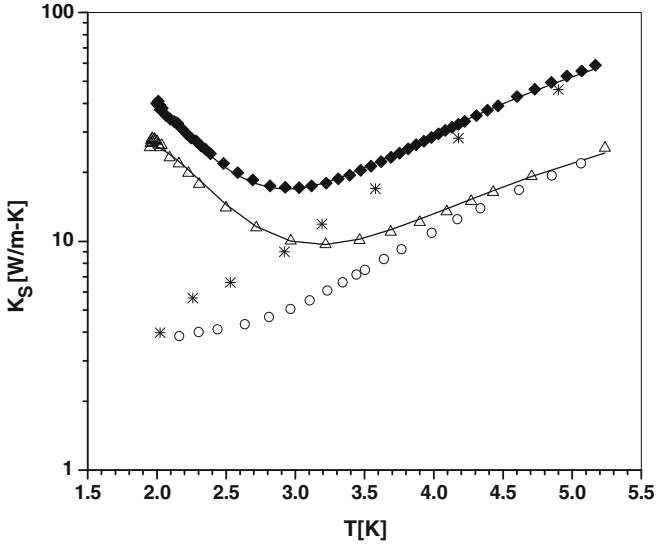

Figure 7. Plot of K_S vs. T. (■) C1 – zero field, (∗) C1 – trapped flux 81 mT, (△) A1 − zero field, (○) A1 − trapped flux 60 mT. Solid lines are the fitting curves of eq. (6).

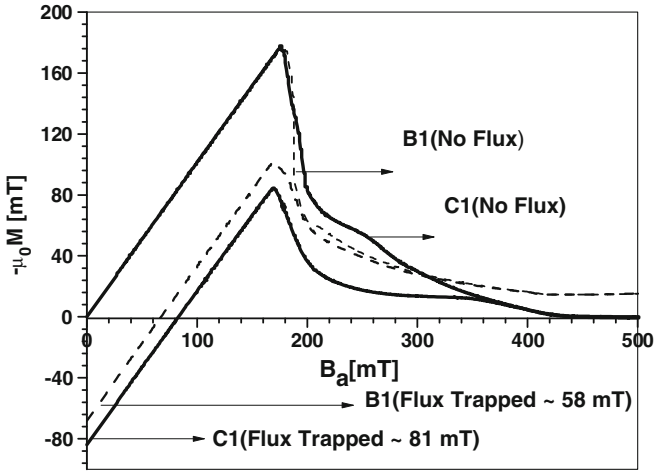

Figure 8. Magnetization curves at $T = 2$ K with and without remnant magnetization for (−−) A1, (—) C1.

used for samples A1 and C1 to calculate the electron mfp. The thermal conductivity model defined in §3 gives a reasonable fit of the experimental data points as shown in figure 9, when corrected using eqs (7) and (8) to take into account the presence of trapped vortices. The error in the calculation of K is $\langle(\Delta K/K)^2\rangle^{1/2} \cong 6\%$. Figure 9 shows that the deviation of the theoretical curve from the experimental data increases with the increase of trapped flux which signifies that other mechanisms, such as inter-vortex tunnelling and collective mode excitations of the flux line lattice, play a role at higher fields.

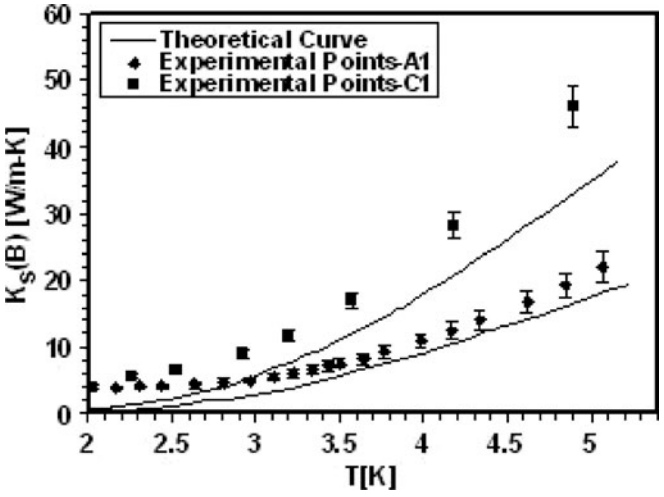

Figure 9. Effect of trapped vortices on the thermal conductivity of the superconducting state in samples A1 and C1. Solid lines represent the qualitative theoretical model by Vinen *et al* at low inductions and low temperature.

As the flux lines act as normal metal cores randomly distributed over the sample cross-section, they can be treated as point-like scattering centres to the thermally excited phonons and BCS quasiparticles. The thermal conductivity results of samples A1 and C1 with trapped vortices are fitted with eq. (9) taking into account that the vortex cores are randomly distributed point-like scattering centres. The fitting parameters in the presence and absence of trapped vortices are summarized in table 2.

From table 2 we can see that the gap parameter α and the coefficient of momentum exchange of electrons with the lattice vibration, A, decrease while the coefficient of momentum exchange of phonons with the electrons, D, increases in the presence of trapped vortices. The parameter $A \propto N^{2/3}$ and the parameter $D \propto N^{-2}$, where N is the effective number of conduction electrons per atom. As the vortices are trapped inside the superconductor, the effective number of conduction electrons reduces because of the bound excitations within the vortex core. The reduction in the gap energy α is due to the low energy excitations close to the vortex core. The energy gap of these excitations is very small and is given by $\varepsilon_0 \sim \Delta_0^2/E_F$. So the effective energy gap will be $\Delta_{eff} \sim (\Delta_0 - \varepsilon_0)$. Taking $E_F = 0.00018 m_0 c^2 = 91.8$ for niobium and $\Delta_0 = 1.86$ (A1) and 1.78 (C1) from the experimental fit data of the zero trapped vortex sample, we get $\varepsilon_0 \sim 0.04$ (A1) and 0.034 (C1) leading to an effective energy gap of $\Delta_{eff} \sim 1.82$ (A1) and 1.74 (C1). This simple explanation gives an error of 2.4% for the fit parameter α.

Figure 10 shows the variation of thermal conductivity with the applied magnetic field for the sample B1 with and without trapped vortices at 2 K. We can see that the value of H_{c1} and H_{c2} are independent of the sample condition from the point of view of trapped vortices. Both the curves are showing the same behaviour in the mixed state. In the mixed state the phonon contribution is negligibly small; it is the electronic contribution which increases with the increasing magnetic field as more and more quasiparticles start contributing to the thermal conductivity. Eventually, as the applied field reaches H_{c2}, the bulk of the superconductor is in the normal state while the surface remains in the superconducting state to an extent of the order of coherence length ξ_0. The figure shows a constant thermal conductivity between H_{c2} and a value of the applied magnetic field beyond the third critical field H_{c3}. So we could not find any effect of the surface sheath on the measured thermal conductivity, as expected. Above H_{c2}, the specimen shows thermal conductivity behaviour of the normal metal. But there is a marked difference of the measured thermal conductivity data in the region $0 \leq H \leq H_{c1}$ for the sample with and without trapped vortices. No magnetic flux enters the samples up to the first

Table 2. Theoretical fitting parameters in the presence and absence of trapped flux lines.

	Sample A1		Sample C1	
Parameters	Zero flux	Trapped flux (58 mT)	Zero flux	Trapped flux (81 mT)
α	1.86	1.78	1.78	1.70
L	2.45×10^{-8}	2.45×10^{-8}	2.45×10^{-8}	2.45×10^{-8}
A	1.00×10^{-5}	1.77×10^{-4}	1.00×10^{-6}	7.94×10^{-5}
$1/D$	402	1216	216	758
B	3.01×10^{3}	3.35×10^{2}	6.32×10^{3}	2.63×10^{2}

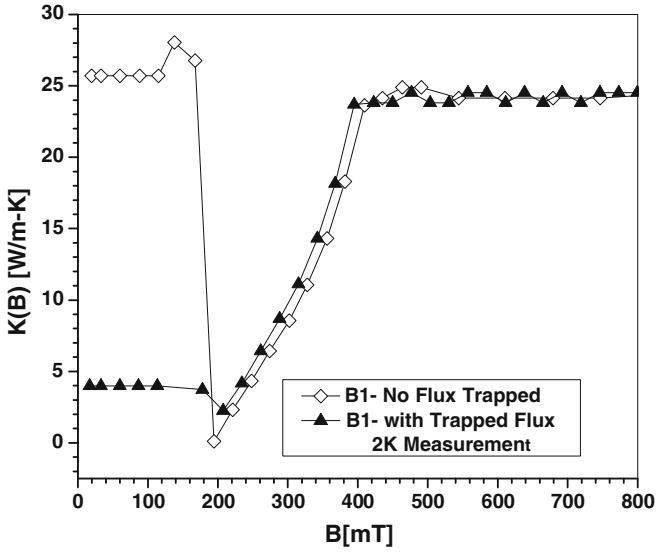

Figure 10. Field dependence of the thermal conductivity with and without trapped vortices measured with the field parallel to the heat flow direction at 2 K.

flux penetration at 180 mT. Below H_{c1}, the difference between the thermal conductivity values of the two curves in figure 10 is due to the strong scattering of phonons by the vortex cores as explained earlier.

At large inductions and low temperature, the field-dependent thermal conductivity is represented by the Houghton–Maki theory described by eq. (9). A plot of μ vs. $\Delta K/K_e^n$ is shown in figure 11.

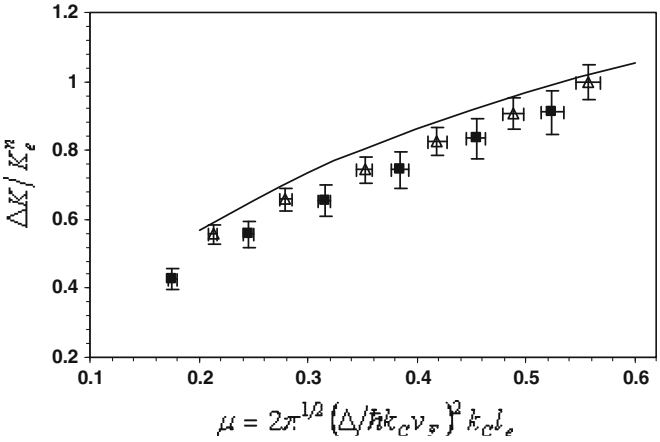

Figure 11. $\Delta K/K_e^n$ as a function of μ in sample B1. (△) Sample B1 without any trapped flux in zero field, (■) sample B1 with an initial remnant magnetization of about 58 mT. Solid line is the theoretical curve of Houghton–Maki.

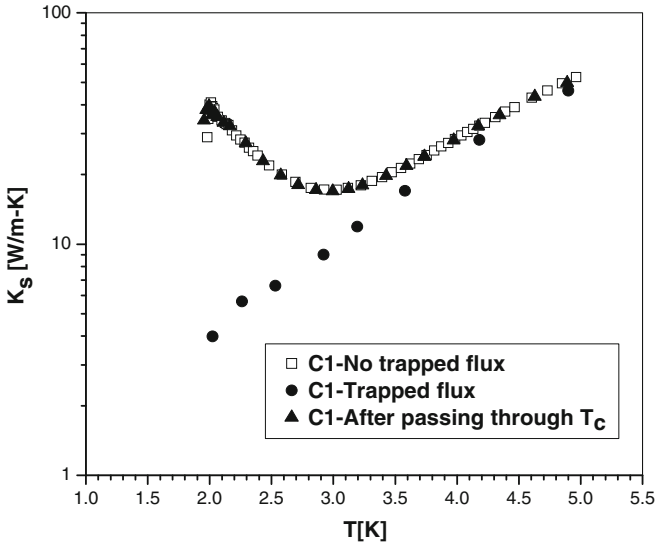

Figure 12. Plot of thermal conductivity in superconducting state in zero remnant field, with remnant field and heating up the sample through T_c to exclude the flux lines to reproduce the zero-field curve.

Figure 11 shows that when there are trapped vortices in zero field, the experimental data points for $0.2 \leq \mu \leq 0.6$ lie below the theoretical curve as well as the baseline measurement data in zero field without the trapped vortices. This might be due to the additional contributions from the bound excitations in the form of tunnelling. Although the exact cause is not yet clear, there is definitely an additional contribution to the thermal conductivity in case of initial remnant magnetization. An experiment can be conducted in future with different remnant magnetizations at zero field and the corresponding thermal conductivity measurement will produce a systematic deviation from the Houghton–Maki theory and the evidence for this new contribution to the thermal conductivity can be established.

Finally, figure 12 shows the measurements of the thermal conductivity of sample C1 after zero-field cooling, after the applied magnetic field was cycled from zero up to H_{c2} and then back to zero, and after warming up the sample above T_c followed by zero-field cooling. The remnant magnetization after cycling the applied magnetic field is about 81 mT. As shown in figure 12, the phonons are strongly scattered by the vortex cores. By raising the temperature of the sample above T_c (9.25 K), the remnant magnetic field is homogeneously distributed throughout the normal conducting sample. By lowering the temperature below T_c, the magnetic flux is expelled from the superconductor and a new thermal conductivity measurement reproduces the data obtained after the first measurement, in the absence of any applied magnetic field.

5. Conclusions

The thermal conductivity as a function of temperature measured on large-grain niobium samples in the Meissner state is well described by the model of ref. [8] within the

experimental error of $\pm 6\%$. The measurements clearly show the presence of a phonon peak at around 2 K. One important observation is that the phonon peak is eliminated by the presence of trapped vortices due to the strong scattering of phonons with vortex cores. When the vortices are trapped inside the sample, the fit parameters indicate a reduction of the gap energy α due to the low energy excitations having a very small energy gap $\sim \Delta_0^2/E_F$ close to the vortex core. Also the effective number of conduction electrons decreases due to the bound excitations in the vortex cores. The dependence of the thermal conductivity with the applied magnetic field for the samples with and without trapped vortices show the same H_{c1} and H_{c2} values as from the magnetization measurement. Finally, when the temperature of the samples is cycled above T_c, the thermal conductivity measured for the sample in the absence of an applied magnetic field is restored. The temperature dependence of the thermal conductivity at low temperature and low magnetic field agrees qualitatively with the model of Vinen *et al*. In the vicinity of H_{c2} the thermal conductivity agrees quite well with Houghton–Maki theory for the virgin sample, i.e without any trapped vortices. But an initial flux is trapped within the sample, the measured thermal conductivity deviates from the Houghton–Maki theory and an increase in thermal conductivity can be observed in the range of $0.2 \leq \mu \leq 0.6$. Future experiments with different initial trapped vortices and subsequent measurement of the thermal conductivity in the range of $0.2 \leq \mu \leq 0.6$ might help to interpret the deviation from the theory.

Acknowledgements

This work was supported by US DOE contract DE-AC05-84ER40150 and Reference Metals Company Inc. CRADA 2004-S002-Mod 2. J Mondal would like to thank Dr L M Gantayet, Director BTDG and D P Chakravarthy, Head APPD, for their keen interest in this program.

References

[1] P Kneisel, G R Myneni, G Ciovati, J Sekutowicz and T Carneiro, *Proc. of the 2005 Particle Accelerator Conference*, Tennessee, TPPT076
[2] P Kneisel, *Proc. of the 13th SRF Workshop* (Peking Univ, China, October 2007) Th102
[3] J Lowell and J B Sous, *Phys. Lett.* **A25**, 469 (1967)
[4] W F Vinen, E M Forgan, C E Gough and M J Hood, *Physica (Utrecht)* **55**, 94 (1971)
[5] Sergei Sergeenkov and Marcel Ausloos, *Phys. Rev.* **B52**, 3614 (1995)
[6] K Maki, *Phys. Rev.* **158**, 397 (1967)
[7] J B Sousa, *Physica (Utrecht)* **55**, 507 (1971)
[8] F Koechlin and B Bonin, *Supercond. Sci. Technol.* **9**, 453 (1996)
[9] A Houghton and K Maki, *Phys. Rev.* **B4**, 843 (1971)
[10] N J Imfeld, W Bestgen and L Rinderer, *J. Low Temp. Phys.* **60**, 223 (1985)
[11] D K Finnemore and D E Mapother, *Phys. Rev.* **140**, A507 (1965)
[12] J Bardeen, G Rickayzen and L Tewordt, *Phys. Rev.* **113**, 982 (1959)
[13] H Padamsee, J Knobloch and T Hays, *RF superconductivity for accelerators* (Wiley, New York, 1998)
[14] C Caroli *et al*, *Phys. Lett.* **9**, 307 (1964); *Phys. Kondens. Mat.* **3**, 380 (1965)
[15] E B Hansen, *Phys. Lett.* **A27**, 576 (1968)
[16] W Bergk and L Tewordt, preprint.
[17] P H Kes, J P M van der Veeken and D De Klerk, *J. Low. Temp. Phys.* **18**, 355 (1975)